Light management in TiO₂ thin films integrated with Au plasmonic nanoparticles

Light management in TiO_2 thin films integrated with Au plasmonic nanoparticles

Matteo Ghidelli[a,b], Luca Mascaretti[a,c], Beatrice Roberta Bricchi[a], Andrea Brognara[a], Tarek Afifi Afifi[a], Valeria Russo[a,d], Carlo Spartaco Casari[a,d], Andrea Li Bassi[a,d]

[a]*Micro- and Nanostructured Materials Laboratory, Department of Energy, Politecnico di Milano, via Ponzio 34/3, 20133, Milano, Italy.*

[b]*Present affiliation: Structure and Nano/-Micromechanics of Materials, Max-Planck-Institut für Eisenforschung GmbH, Max-Planck-straße 1, 40237 Düsseldorf, Germany.*

[c] *Present affiliation: Regional Centre of Advanced Technologies and Materials, Faculty of Science, Palacký University Olomouc, Šlechtitelů 27, 783 71, Olomouc, Czech Republic.*

[d]*Center for Nanoscience and Technology – IIT@Polimi, via Giovanni Pascoli 70/3, 20133, Milano, Italy.*

Abstract

The light-harvesting properties of metal oxide thin films can be remarkably increased by the introduction of plasmonic nanostructures, leading to higher efficiencies in photovoltaic or photoelectrochemical devices. In the prototypical material combination, Au-TiO_2, nano- and mesoscale porosity of TiO_2 is desirable to improve not only the light-harvesting, but also the available surface area for chemical reactions. Moreover, great attention has been given to the control of size and shape of Au nanoparticles (NPs) to increase the overall optical properties of the film. In this work, we investigate the optical properties of the composite Au-TiO_2 films exhibiting remarkable light scattering properties. TiO_2 is characterized by a tree-like hierarchical morphology produced by pulsed laser deposition, and two different configurations for Au integration, namely Au on top and at the bottom of TiO_2 are explored by varying the size of Au NPs. The hierarchical oxide morphology allow to achieve superior scattering properties after the combination with Au NPs with respect to films obtained from a commercial paste

deposition. Both the Au-top and Au-bottom configurations enable to tune the plasmonic properties of Au NPs. Specifically, outstanding scattering properties are exhibited by the composite TiO_2 film grown on top of large (~100 nm) Au NPs. These results show the potential interest of employing such integrated films as photoanodes in dye-sensitized or perovskite-based solar cells, or in photoelectrochemical cells for water splitting. An analogous approach can be employed for alternative materials, both considering the plasmonic structures as well as the semiconductor layer.

1. Introduction

Plasmonic metal nanoparticles (NPs) are known for their unique ability to strongly enhance nanoscale light-matter interactions via free electron excitations triggered by specific light wavelengths, resulting in a characteristic localized surface plasmon resonance (LSPR) [1,2]. Beyond known decorative aspects [2,3], the use of plasmonic resonances has tremendously developed [4,5], enabling the manipulation of light in wide research directions that crosscut many applications including sensors [6] and biosensors [7], medical therapy [8], photodetectors [9], photochemistry [10], as well as surface enhanced Raman spectroscopy (SERS) [11]. The precise tailoring of the LSPR wavelength – necessary for the aforementioned applications – can be achieved by controlling the average size and shape of NPs, as well as the interparticle spacing [2,12]. In particular, the integration of plasmonic NPs in semiconductors is considered a particularly promising approach for extending and/or improving their light absorption for solar energy harvesting technologies, including photocatalysis [13], photovoltaics [14,15], and photoelectrochemical (PEC) hydrogen production [16].

In the aforementioned applications, wide-bandgap semiconductor oxides (such as TiO_2 and ZnO) have a key role and their integration with plasmonic NPs can give rise to several effects, leading to the overall device improvement. In PEC cells, photoanodes (*n*-type semiconductors) or photocathodes (*p*-type) play the active role of photocurrent generation upon light absorption. Plasmonic NPs can induce, for instance, hot carrier injection

to allow a visible-light sensitization [17–19] or scattering effects, promoted by relatively large NPs (> 50 nm), to allow a more efficient UV absorption [20,21]. In thin-film solar cells, Al-doped ZnO (AZO) thin films integrated with plasmonic NPs can be employed as plasmonic back-reflectors (PBRs) to enhance the light absorption in the active layer of the device [22,23]. In dye-sensitized or perovskite solar cells, mesoporous TiO_2 photoanodes provide light-harvesting and electron transport from the active layer to the back-contact; the former property can be significantly enhanced by the introduction of plasmonic NPs, increasing the solar cell efficiency [24–27]. In this regard, several works report the use of chemical methods to integrate the mesoporous photoanode with NPs exhibiting a core-shell [24,25,28] or complex [26] morphology, or with different loadings of NPs [27]. Subsequently, the photoanode is deposited by doctor-blade [24], screen-printing [25], or spin-coating techniques [26–28], which do not generally allow its fine morphological tuning. Conversely, physical vapor deposition (PVD) methods, such as sputtering or evaporation, allow the integration of plasmonic NPs at the bottom, on top, or within the oxide film [19,20,23,29]. A heat treatment can be further employed to tune the NP plasmonic resonance; however, these approaches present limitations in the micro- and nanoscale morphology of the semiconductor, which is generally compact [19,23,29].

Pulsed Laser Deposition (PLD) can be considered as a highly flexible synthetic method that could potentially address the aforementioned issues [30–32]. Indeed, hierarchically-organized films of different oxides with tunable optical and electrical properties can be obtained by playing with the process parameters, and their superior functional properties have already allowed their application as photoanodes in dye-sensitized [33–35] or perovskite-based [36] solar cells and in PEC water splitting [37]. This technique also allows the preparation of plasmonic Au NPs with a precise tuning of their average size and coverage, thus leading to a control on their optical properties [38,39]. Furthermore, a PLD co-deposition process can be exploited to realize porous TiO_2 layers integrated with Au NPs homogeneously dispersed through the film volume [40,41]. As a consequence, the advantages of this approach could pave the road towards novel photoanodes by combining plasmonic NPs and hierarchical oxide films with enhanced light harvesting properties [42,43].

In this work, we propose a combined vapor phase approach for the integration of Au NPs within TiO_2 films, based on the tuned synthesis of TiO_2 nanostructured porous films by PLD and the integration with Au NPs produced by thermal evaporation or PLD. Specifically, we focus on two different integration strategies involving the deposition of Au NPs of different size on top and at the bottom of nanostructured TiO_2 films, representing two alternative approaches for the optical management in photoanodes. Specifically, in the first configuration Au can penetrate down to about 100 nm below the TiO_2 surface and subsequent thermal annealing promotes Au diffusion, while also managing to tune the LSPR wavelength by favoring Au NPs growth and separation; light scattering is promoted for larger NPs. In the second configuration, the growth and morphology of TiO_2 nanostructures are influenced by the size of the underlying Au NPs, with size in the range ~25-100 nm, leading to enhanced light scattering properties dictated by the synergetic effect of the plasmonic properties of Au NPs and the organization/spacing of the TiO_2 nanostructures. In both cases, we show that the optical response of the composite Au/TiO_2 films can be controlled to a superior extent with respect analogous ones obtained from a commercial TiO_2 paste, especially in terms of light scattering.

2. Experimental methods

The PLD conditions to deposit nanostructured TiO_2 film are extensively described elsewhere [40]. Here, a TiO_2 (99.9% pure) target was ablated with a ns-pulsed laser (Nd:YAG, 2nd harmonic, λ = 532 nm, pulse duration 5-7 ns, 10 Hz repetition rate, fluence on the target 3.5 J/cm^2). Films were deposited on Si (100) and soda-lime glass substrates mounted on a sample holder at a fixed target-to-substrate distance of 50 mm. Depositions were performed at room temperature with a pure O_2 background gas at a fixed 8 Pa pressure. Au NPs were obtained by depositing a Au layer by thermal evaporation, followed by thermal dewetting to induce formation of NPs having an average size directly related to the layer thickness. Au grains (99.9% purity) were evaporated in an Edwards E306 thermal evaporator (starting from a base vacuum level of ~$2\cdot10^{-5}$ mbar) controlling the Au equivalent thickness by means of a quartz microbalance. The equivalent thickness information for the specific

samples is provided in the Results and Discussion Section. Post-deposition annealing treatments of TiO_2 and Au were performed in air in a Lenton muffle furnace with 4 °C/min heating ramp and 2 hours dwell at 500 °C. These conditions enable both the crystallization of TiO_2 in anatase form and the formation of Au NPs exploiting dewetting phenomena of the Au films. Specifically, for the TiO_2/bottom Au NP layers the following synthesis sequence was employed: Au deposition - Au NP formation by thermal dewetting - TiO_2 deposition over the NP - thermal annealing of the whole system; for the top Au NP/TiO_2 layers: TiO_2 deposition - Au deposition over the TiO_2 layer - thermal annealing of the whole system.

The integration of Au with commercial TiO_2 paste was carried out as a comparison with nanostructured TiO_2 films by PLD. A TiO_2 commercial paste (Dyesol 18NR-T) composed of anatase nanoparticles with average diameter of 20 nm was diluted in ethanol and deposited by doctor blade technique, followed by thermal annealing at 500°C in air to allow solvent evaporation and sintering among nanoparticles.

A field emission scanning electron microscope (FEG-SEM, Zeiss Supra 40) was used to perform morphological characterization analyzing films deposited on Si (100) substrate and to determine the Au NP size distribution by image analysis with Image J software. Optical transmittance spectra were evaluated with a UV-vis-NIR PerkinElmer Lambda 1050 spectrophotometer with a 150 mm-diameter integrating sphere in the range 250–2000 nm, illuminating the sample from the glass substrate side. All the acquired spectra were normalized with respect to glass substrate contribution.

3. Results and discussion

3.1 Au nanoparticles at the bottom of TiO_2 layer

The first investigated composite film configuration consists of a layer of Au NPs deposited on the transparent substrate (glass in this case), over which a nanoporous TiO_2 layer is then deposited. This represents the situation in which plasmonic nanoparticles are deposited at the bottom of the photoanode, i.e. at the

interface with the underlying electrode substrate, enhancing light trapping via scattering effects. This configuration offers a potential interest for an increased light utilization in dye-sensitized [24,25] or perovskite-based [26,27] solar cells, as well as in PEC water splitting cells [20,21].

Plasmonic NPs favor scattering effects especially when their size is in the range of several tens nm [15]. In order to achieve and tune the desired NP dimensions, we evaporated Au layers with a different nominal thickness, namely 2.5, 5 and 10 nm. An annealing treatment in air at 500 °C was then performed to promote the layer dewetting and formation of irregular nanoparticles (NPs) [38]. The so-obtained Au NPs were characterized by an average size of ~23 ± 7 nm, ~50 ± 22 nm and ~100 ± 45 nm, respectively (Fig.1), and by a very large aspect ratio (i.e. they are quite 'flat' - see Figs. 2 and 4 as well as Ref. [38]).

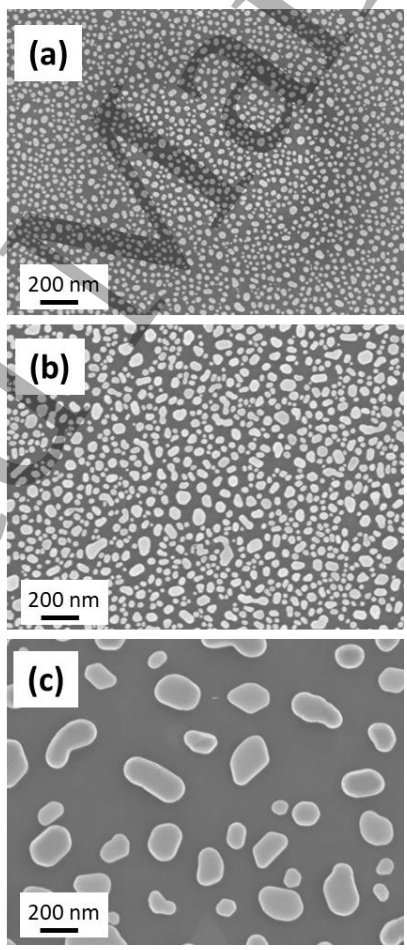

Figure 1 - SEM images of Au NPs obtained after dewetting of evaporated Au layers. Different average sizes, i.e. 23, 50, and 100 nm are reported in (a), (b), and (c), respectively.

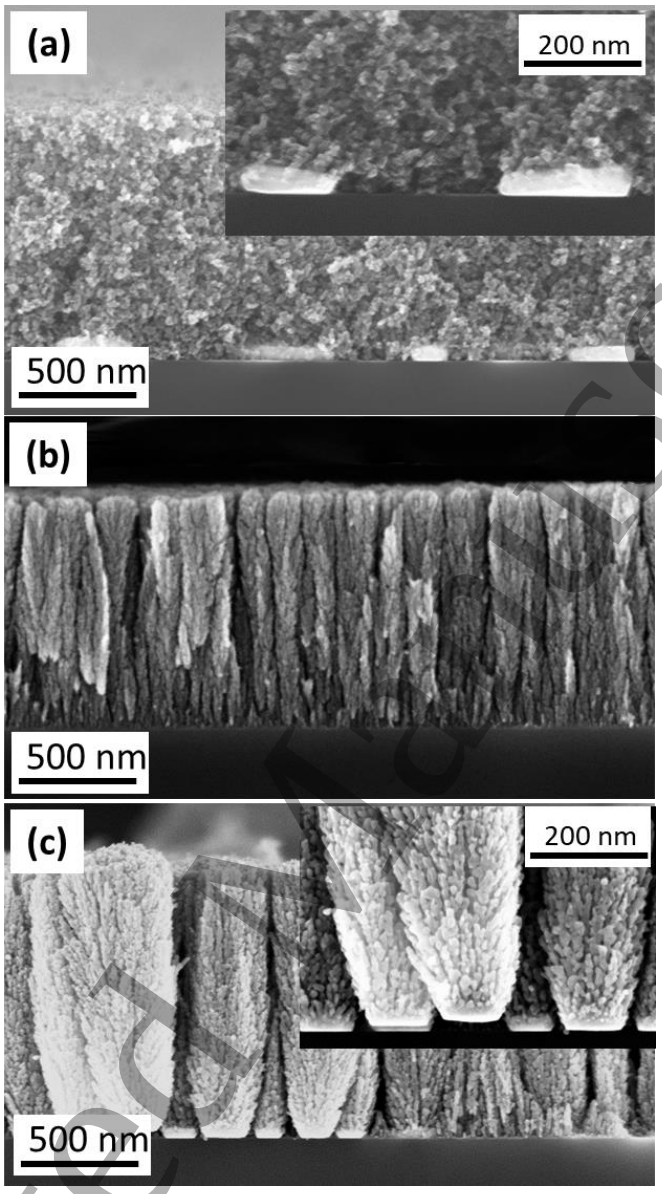

Figure 2 – SEM images of TiO_2 paste (a), PLD TiO_2 (b) and PLD TiO_2 grown on 100 nm size Au NPs on bottom (c).

A nanoporous TiO_2 layer was then deposited over the Au NPs; Fig. 2 shows cross-sectional SEM images for the case of 100 nm Au NPs. We compare the morphological properties of a conventional nanoparticle-assembled film (Fig. 2a), obtained by depositing a commercial anatase paste (TiO_2 NPs average size 20 nm) by doctor blade (used here as reference), to those of a hierarchically-nanostructured film (Fig. 2b), deposited by PLD. While the former exhibits a nanoporous morphology with a random assembly of TiO_2 nanocrystals, the latter shows a

multiscale porosity and hierarchical organization in the form of 'nanotrees' (see Fig. 2b, showing a PLD TiO_2 film grown on a bare Si substrate. This is a well-known feature of PLD-deposited hierarchical films, which favors light diffusion and a large specific surface area, as thoroughly discussed previously [33,35,42,43]. This morphology occurs when the background pressure is large enough to favor gas-phase cluster nucleation, but without promoting significant scattering and diffusion of clusters before reaching the substrate. These conditions lead to a ballistic deposition of a highly direction flux of clusters with relatively low kinetic energy, promoting the nanotree growth [44]. In Fig. 2c, notably, we observe that Au NPs work as nucleation centers for the growth of nanotrees (Fig. 2b), with a basis width determined by the NP size. This results in wider, well-defined and more separated TiO_2 trees compared to those that grow on a bare substrate (i.e. without Au NPs, Fig. 2b), while suggesting a viable strategy to control the trees shape and organization by properly tuning the NP size. A second annealing step in air at 500 °C was then exploited to induce crystallization of the TiO_2 layer to the anatase phase, as discussed in previous works [33,35] and confirmed by Raman spectroscopy (not shown).

We then compare the optical properties of the different TiO_2 layers (paste and nanotrees) with and without Au NPs at the bottom (Fig. 3). Transmittance curves (Fig. 3a) show that above the anatase bandgap (3.2 eV, i.e. ~380 nm) the bare TiO_2 layers have a quite large transparency, but slightly smaller for the hierarchical layer, which is characterized by defined interference fringes related to multiple reflections in the film. When TiO_2 is deposited on top of the Au NPs, the transmittance decreases, which can be ascribed to increased absorption and/or reflectance. A wide absorption feature is now visible, extending from ~500 nm up to above 1500 nm, which is due to the localized surface plasmon resonance (LSPR) of the Au NPs (see comments to Fig. 5 below).

Fig. 3b shows the haze factor of the investigated TiO_2/Au layers, defined as the diffuse-to-total transmittance ratio (diffuse meaning not along the incident direction) [45], which can be considered as an indication of the light scattering capability of the system. It can be observed that the plasmonic behavior of Au NPs enhances haze in the case of TiO_2 paste, while the interplay between Au NPs and hierarchical TiO_2 provides an overall superior scattering ability.

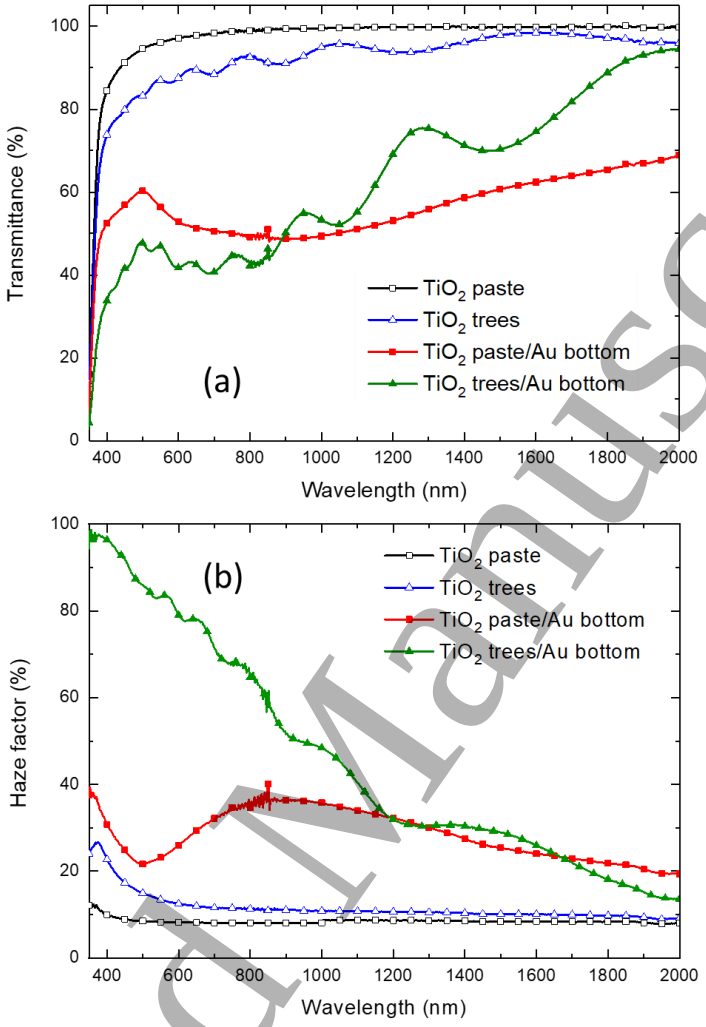

Figure 3 – Comparison of the optical transmission spectra (a) and of the haze factor (b) of TiO_2 trees and paste with 100 nm Au NPs on bottom.

For this reason, in the following we focus our study on the integration of Au NPs with tuned size and thus optical properties in PLD hierarchical TiO_2 films only. We thus varied the average size of NPs at the bottom of the TiO_2 film, by changing the nominal thickness of the evaporated Au layer before the dewetting process. This enables to obtain smaller Au NPs, although characterized by a similar shape and aspect ratio (see Fig. 1b,c). Fig. 4 shows SEM images of PLD hierarchical TiO_2 films deposited on top of 23 nm and 50 nm Au NPs (average size);

comparison with Fig. 2c confirms that the NPs act as nucleation centers affecting the tree growth and shape/separation.

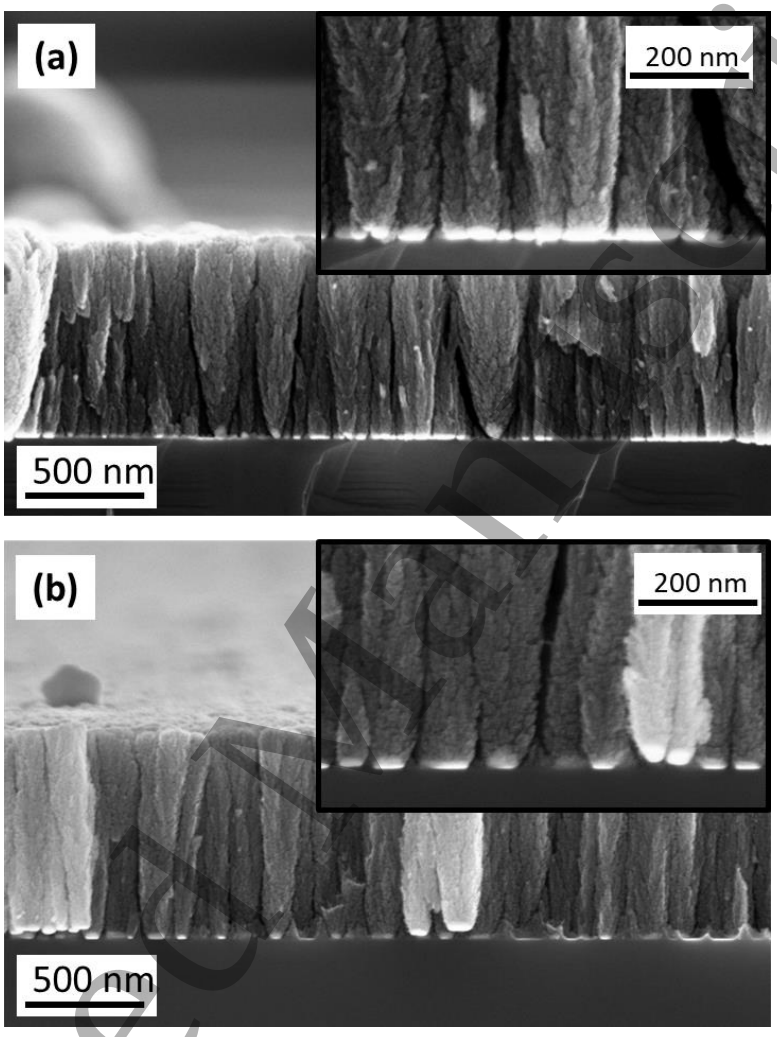

Figure 4 – SEM images of nanostructured TiO_2 films with Au NPs of 23 nm (a) and 50 nm (b) at the bottom.

More interestingly, the optical properties show a dependence on the underlying size distribution of Au NPs (Fig. 5). Transmittance curves in Fig. 5a show that the bare glass/Au NP systems (i.e. before TiO_2 deposition) are characterized by a plasmonic absorption peak that blueshifts upon reducing the NP size, i.e. centered at ~540 nm for the 23 nm-size NP and at ~600 nm for the 50 nm-size NP. On the other hand, large NPs (100 nm) exhibit a broad absorption extending in the near IR up to 2000 nm [46,47]. The Au NP plasmonic features consequently affect the transmittance spectra of the TiO_2/Au NP layers, overlapping to the oxide film absorption edge and

interference fringes. Accordingly, the haze factor can be modulated by adjusting the NP size, as shown in Fig. 5b, where the largest NP provide the highest haze factor. Specifically, the TiO_2/Au film with 100 nm-NPs exhibits an outstanding haze factor, i.e. > 50% in the whole visible range (380−780 nm). Such enhancement was not achieved by the corresponding TiO_2/Au system obtained from a commercial TiO_2 paste (Fig. 3b). This effect may be ascribed to a strong light-trapping mechanism mediated by the growth of tree-like nanostructures on top of large Au NPs.

Previous investigations reported a similarly high haze factor (> 30% in the visible range) by SiO_2@Ag NPs at the bottom of a TiO_2 photoanode, which led to an enhancement of 38% of the short-circuit current for 7 µm-thick dye-sensitized solar cells [25]. Indeed, the LSPR in relatively large NPs decays mainly radiatively, leading to scattering effects with low parasitic absorption, i.e. light absorption in the NPs instead of in the active layer or photoanode layer of the solar cell. Accordingly, effective plasmonic back-reflectors for thin-film solar cells can be obtained by employing large and well-separated NPs, similarly as those in Fig. 1c, leading to high scattering and low parasitic absorption [23]. Thus, the high fraction of scattered light by the TiO_2/Au films (especially the one with 100 nm NPs), employed as photoanodes, could be effectively absorbed by a dye/perovskite material as active component in a solar cell. On the other hand, in light of applying the TiO_2/Au composite layers as photoanodes in PEC water splitting experiments (with back-illumination), a modification by doping/hydrogenation of TiO_2 would be required to make use of the scattered photons in the visible wavelengths [48,49]. Alternatively, an additional semiconductor with lower bandgap, such as hematite (α-Fe_2O_3), could be placed on top of the device [20]; this may further increase the performance due to heterostructure formation [50].

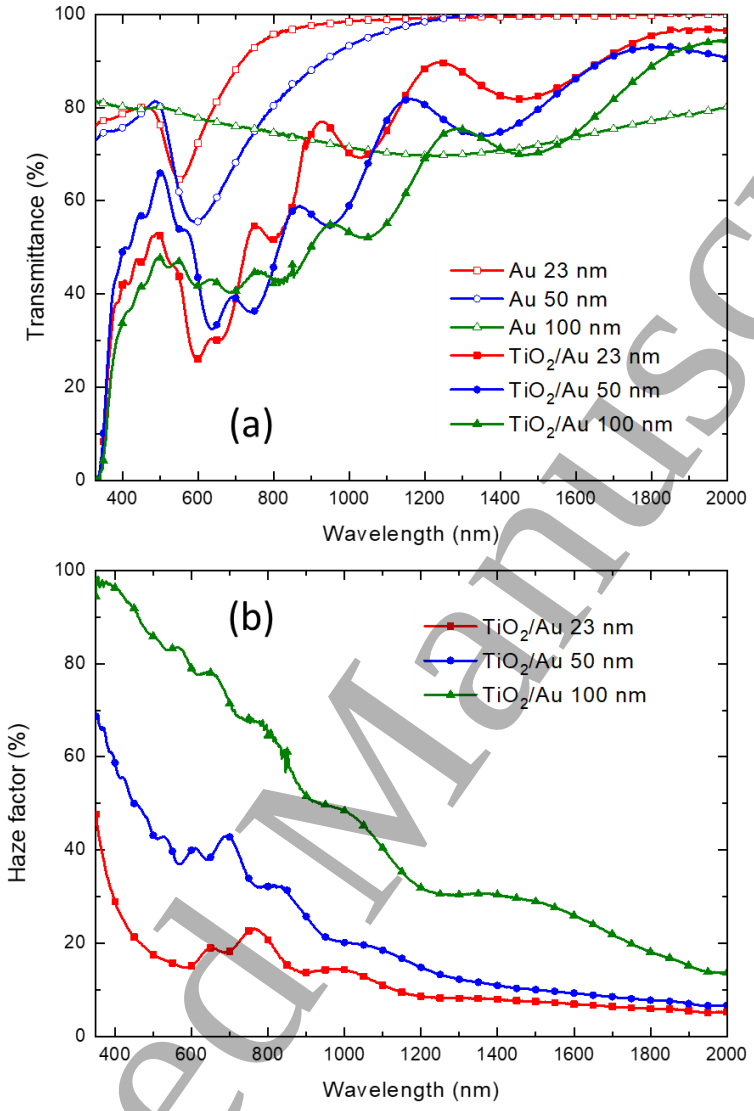

Figure 5 – Optical transmittance (a) and haze factor (b) of nanostructured TiO_2 films with different size of Au NPs (23, 50, and 100 nm) at the bottom.

3.2 Au nanoparticles on top of TiO_2 surface

The opposite approach consists in the deposition of Au NPs *on top* of the surface of the TiO_2 layer. In this case, the aimed functionality of the metal NP layer can be twofold. First, it can act as a scattering layer in order

to promote light trapping in the film. This configuration represents an alternative or complementary approach with respect to the case of the NPs at the bottom of TiO_2, depending on the specific application and the foreseen illumination geometry (from the top/bottom). Second, evaporation of Au from the meso- or nanoporous TiO_2 top surface can be considered as a means to *infiltrate* Au NP in the top oxide layer, and thus *decorate* not only the top surface, but possibly also part of the internal TiO_2 surface, consequently leading to the integration of plasmonic nanostructures within the oxide film. This intimate contact between the two materials can be interesting to exploit plasmonic effects able to realize oxide-based photoanodes with extended photo-response and quantum efficiency to the visible range (such as hot electron injection from the metal NP to the oxide conduction band [17–19]). This infiltration is usually difficult in TiO_2 pastes where porosity is limited to the nanoscale, but can be more feasible in a multiscale-porous system such as the PLD nanotrees [35]. This represents an alternative to other approaches to the synthesis of Au-TiO_2 systems involving e.g. co-deposition strategies, as discussed in our previous work [40].

We therefore evaporated different amounts of Au (i.e. corresponding to a different nominal thickness as measured by quartz microbalance, namely 3, 6, and 15 nm) on top of the PLD hierarchical films and then performed annealing (500°C in air) in order to induce at the same time TiO_2 crystallization to anatase phase and Au dewetting, with the NP size being ruled by the amount of evaporated Au [51,52].

Fig. 6 shows SEM cross-sectional images of TiO_2 films with Au evaporated on top, as deposited (left column, Figs. 6a, 6c, and 6e) and after thermal dewetting (right column, Figs. 6b, 6d, and 6f). The penetration of NPs appears to be limited (of the order of about 100 nm), while the average size of the obtained Au NPs increases with the amount of evaporated Au. A statistical analysis based on top-view SEM images allows to obtain the average Au nanoislands size after thermal dewetting for the different samples, i.e. 12 ± 5 nm (b), 23 ± 12 nm (d), and 115 ± 89 nm (f).

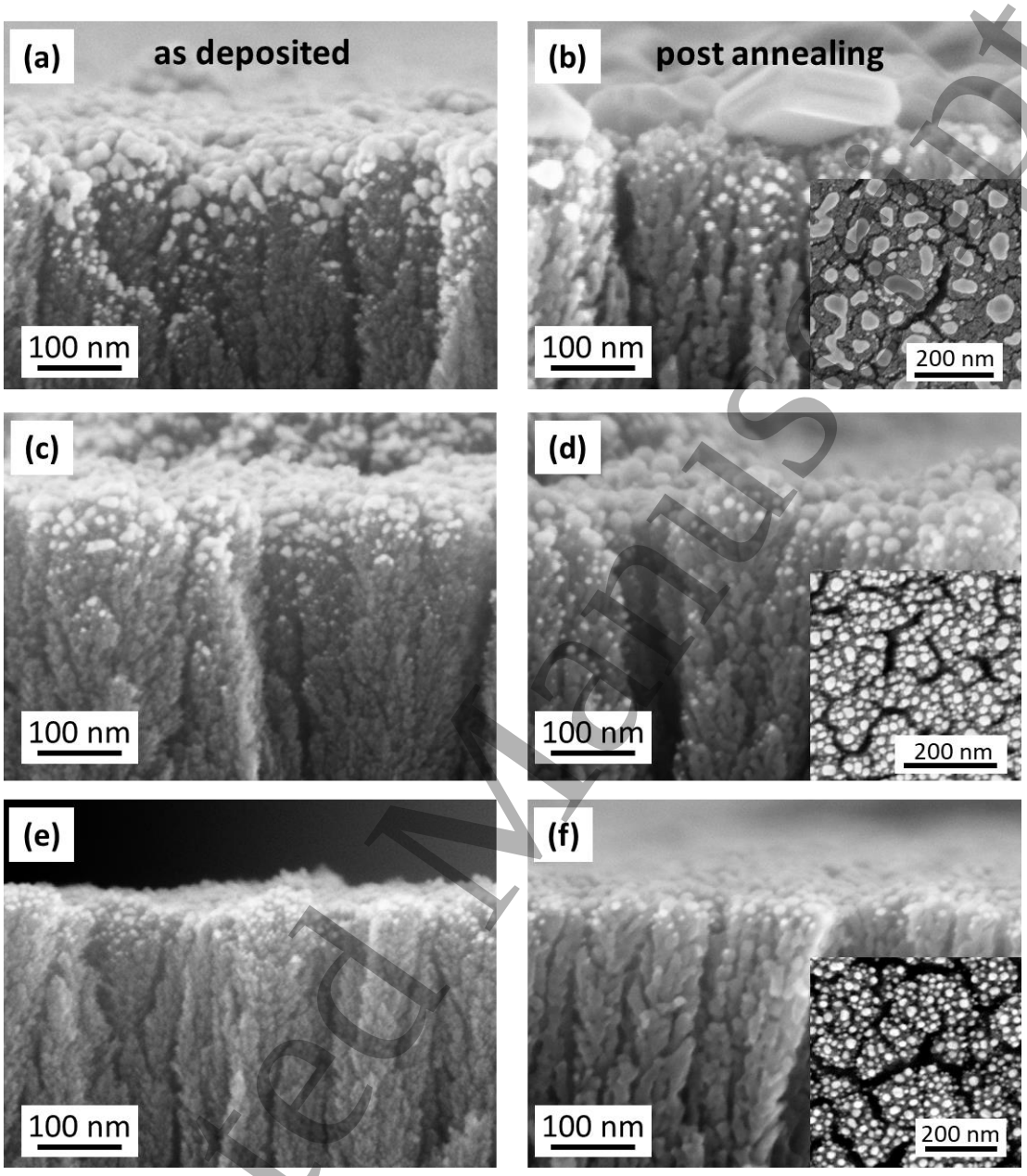

Figure 6 – Nanostructured TiO_2 films with an evaporated Au top-layer of 15 nm (a), 6 nm (c), and 3 nm (e). The effect of the annealing treatment is reported in (b), (d), and (f), highlighting the formation of NPs.

Fig. 7a reports the transmittance spectra of the investigated Au/TiO_2 systems for the different NP dimensions, both for the as-deposited and the annealed samples. Upon annealing (and thus NP coalescence) it is possible to observe the narrowing and the blueshift of the broad absorption feature, which is related to NP

growth. For annealed samples, the peak position redshifts as a function of increasing NP size, starting from less than 600 nm for the smallest NP, while for the largest NPs the absorption band is broad and extends up to ~1000 nm, while the total transmittance of the layer decreases with NP size. Finally, the haze factor is strongly enhanced by the deposition of 115 nm-size Au NPs, consistent with the strong scattering cross section of large plasmonic NP (Fig.7b) [12].

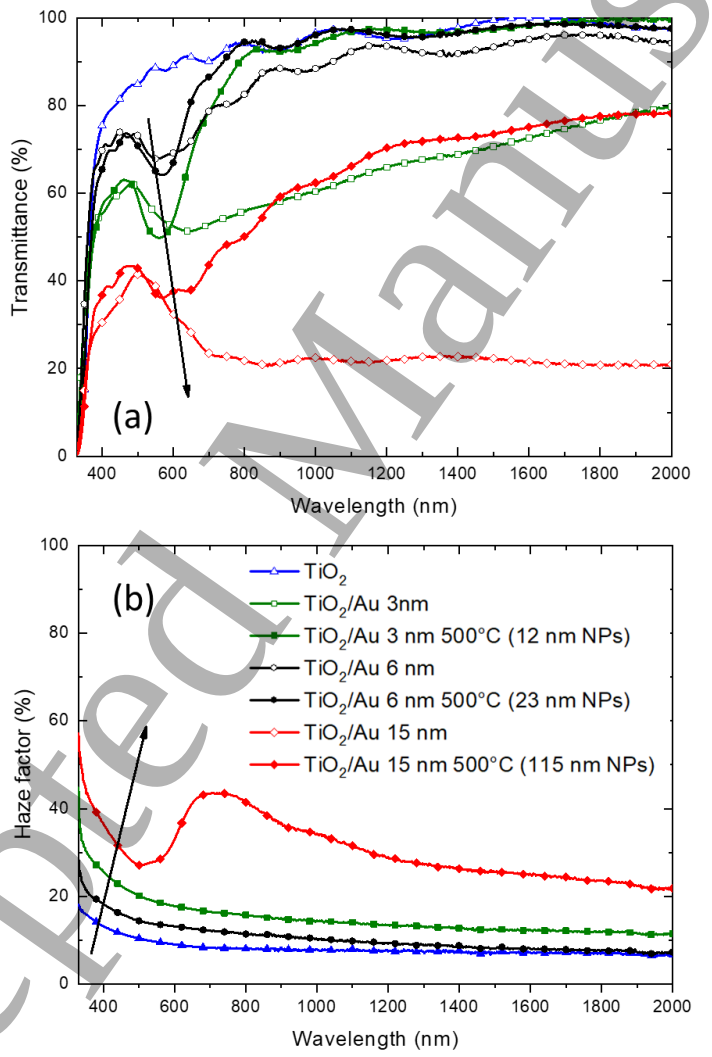

Figure 7 – (a) Optical transmittance spectra of TiO_2 films coated with different Au nominal thicknesses, before and after annealing. (b) Haze factor for Au on top of TiO_2 films after annealing. The legend is unique for panel (a) and (b). The arrows indicate the trend in optical properties as a function of Au amount.

Compared to the configuration with Au NPs at the bottom (Fig. 5b), we clearly observe lower values of the haze factor (Fig. 7b). This may be ascribed to the different morphological properties of NPs obtained in the two cases (Figs. 1, 2, and 4 vs. Fig. 6) and to the different optical path length for the transmittance measurements. Considering a back-side illumination (i.e. from the glass substrate), in the TiO_2/Au configuration (Fig. 5) light first travels through Au NPs and then TiO_2, while in the Au/TiO_2 case (Fig. 7) the opposite occurs. For large plasmonic NPs at the interface between two media, preferential scattering occurs towards the medium with the higher refractive index [53]; as a consequence, a higher fraction of scattered light would travel from the Au NPs to the top surface of the composite film in the TiO_2/Au configuration (Fig. 5b) than in the Au/TiO_2 configuration (Fig. 7b). Thus, the TiO_2/Au film with large NPs may be more suitable as highly-scattering photoanode for solar cell application than the Au/TiO_2 one.

On the other hand, the Au/TiO_2 configuration with smaller NPs (i.e. 12 and 23 nm) may allow to exploit other plasmonic phenomena to increase the quantum efficiency of the final devices. For instance, 'popcorn-shaped' Au NPs dispersed in a mesoporous TiO_2 film [26] and spherical Au NPs combined with TiO_2 nanofibers [54] allowed hot electron injection effects in the so-obtained composite photoanodes. The overall performance of the corresponding perovskite-based solar cells considerably increased. On the other hand, the same effect has been widely exploited in Au-TiO_2 photoanodes in PEC water splitting experiments [17–19], in which Au NPs are conveniently located close to the semiconductor-liquid junction, i.e. at the active surface of the device.

Conclusions

In this work we have shown and discussed how the integration of Au NPs with controlled size and distribution on top or at the bottom of hierarchically organized nanoporous TiO_2 layers can lead to the realization of composite films whose optical properties can be tuned in terms of plasmonic and light scattering behavior. Specifically, the following conclusions can be drawn:

- For nanoporous TiO_2 layers grown on top of a substrate covered with Au NPs, we observe that the average TiO_2 'nanotree' width and film organization are determined by the size of the Au NPs. Furthermore, we show that the LSPR can be tuned by increasing the size of Au NP size from about 25 up to 100 nm. The resulting light scattering properties are dictated by the combination of the size of the NPs and the organization/spacing of the TiO_2 nanostructures.
- For Au NPs grown on top of the nanoporous TiO_2 layers obtained by PLD, we show that the penetration depth is of the order of about 100 nm below the TiO_2 surface, while thermal annealing promotes Au diffusion and tuning of the LSPR wavelength by favoring Au NPs growth. Specifically, we show that the LSPR can be tuned depending on the size of Au NPs. Furthermore, we show that large NPs lead to strong light scattering and haze factor.

Both strategies demonstrate superior optical properties with respect to Au NPs deposited on top/bottom of TiO_2 commercial pastes, indicating the potential for the investigated TiO_2 nanotree + Au configuration for applications in dye-sensitized, perovskite-based, and photoelectrochemical cells. The same materials may be further employed in additional fields of research, such as photocatalysis or sensors, in which highly tunable optical properties are of interest. The two presented approaches (NPs on top/bottom of TiO_2) can be in principle combined together in a single Au/TiO_2/Au system to further extend the range of achievable optical behavior, with other Earth-abundant photoactive semiconductors, i.e. α-Fe_2O_3, or exploited for the realization of alternative plasmonic materials (i.e. transition metal nitrides/semiconductor combinations).

Acknowledgements

The authors wish to acknowledge the FARB project of the Department of Energy, Politecnico di Milano, for financial support. M. Ghidelli acknowledges funding by the Polimi International Fellowship programme.

References

[1] J.A. Schuller, E.S. Barnard, W. Cai, Y.C. Jun, J.S. White, M.L. Brongersma, Plasmonics for extreme light concentration and manipulation, Nat. Mater. 9 (2010) 193–204. https://doi.org/10.1038/nmat2630.

[2] V. Amendola, R. Pilot, M. Frasconi, O.M. Maragò, M.A. Iatì, Surface plasmon resonance in gold nanoparticles: a review, J. Phys.: Condens. Matter. 29 (2017) 203002. https://doi.org/10.1088/1361-648X/aa60f3.

[3] D.J. Barber, I.C. Freestone, An Investigation of the Origin of the Colour of the Lycurgus Cup by Analytical Transmission Electron Microscopy, Archaeometry. 32 (1990) 33–45. https://doi.org/10.1111/j.1475-4754.1990.tb01079.x.

[4] M.L. Brongersma, N.J. Halas, P. Nordlander, Plasmon-induced hot carrier science and technology, Nat. Nano. 10 (2015) 25–34. https://doi.org/10.1038/nnano.2014.311.

[5] A. Naldoni, V.M. Shalaev, M.L. Brongersma, Applying plasmonics to a sustainable future, Science. 356 (2017) 908–909. https://doi.org/10.1126/science.aan5802.

[6] M. Li, S.K. Cushing, N. Wu, Plasmon-enhanced optical sensors: a review, Analyst. 140 (2015) 386–406. https://doi.org/10.1039/C4AN01079E.

[7] J.-F. Masson, Surface Plasmon Resonance Clinical Biosensors for Medical Diagnostics, ACS Sens. 2 (2017) 16–30. https://doi.org/10.1021/acssensors.6b00763.

[8] N.G. Khlebtsov, L.A. Dykman, Optical properties and biomedical applications of plasmonic nanoparticles, J. Quant. Spectrosc. Radiat. Transfer. 111 (2010) 1–35. https://doi.org/10.1016/j.jqsrt.2009.07.012.

[9] H. Chalabi, D. Schoen, M.L. Brongersma, Hot-Electron Photodetection with a Plasmonic Nanostripe Antenna, Nano Lett. 14 (2014) 1374–1380. https://doi.org/10.1021/nl4044373.

[10] Y. Zhang, S. He, W. Guo, Y. Hu, J. Huang, J.R. Mulcahy, W.D. Wei, Surface-Plasmon-Driven Hot Electron Photochemistry, Chem. Rev. 118 (2018) 2927–2954. https://doi.org/10.1021/acs.chemrev.7b00430.

[11] N.R. Agarwal, F. Neri, S. Trusso, A. Lucotti, P.M. Ossi, Au nanoparticle arrays produced by Pulsed Laser Deposition for Surface Enhanced Raman Spectroscopy, Appl. Surf. Sci. 258 (2012) 9148–9152. https://doi.org/10.1016/j.apsusc.2011.12.030.

[12] V. Amendola, O.M. Bakr, F. Stellacci, A Study of the Surface Plasmon Resonance of Silver Nanoparticles by the Discrete Dipole Approximation Method: Effect of Shape, Size, Structure, and Assembly, Plasmonics. 5 (2010) 85–97. https://doi.org/10.1007/s11468-009-9120-4.

[13] A. Naldoni, F. Riboni, U. Guler, A. Boltasseva, V.M. Shalaev, A.V. Kildishev, Solar-Powered Plasmon-Enhanced Heterogeneous Catalysis, Nanophotonics. 5 (2016) 112–133. https://doi.org/10.1515/nanoph-2016-0018.

[14] K. Ueno, T. Oshikiri, Q. Sun, X. Shi, H. Misawa, Solid-State Plasmonic Solar Cells, Chem. Rev. 118 (2018) 2955–2993. https://doi.org/10.1021/acs.chemrev.7b00235.

[15] K. Chan, M. Wright, N. Elumalai, A. Uddin, S. Pillai, Plasmonics in Organic and Perovskite Solar Cells: Optical and Electrical Effects, Adv. Opt. Mater. 5 (2017) 1600698. https://doi.org/10.1002/adom.201600698.

[16] L. Mascaretti, A. Dutta, Š. Kment, V.M. Shalaev, A. Boltasseva, R. Zbořil, A. Naldoni, Plasmon-Enhanced Photoelectrochemical Water Splitting for Efficient Renewable Energy Storage, Adv. Mater. 31 (2019) 1805513. https://doi.org/10.1002/adma.201805513.

[17] Y.-C. Pu, G. Wang, K.-D. Chang, Y. Ling, Y.-K. Lin, B.C. Fitzmorris, C.-M. Liu, X. Lu, Y. Tong, J.Z. Zhang, Y.-J. Hsu, Y. Li, Au Nanostructure-Decorated TiO2 Nanowires Exhibiting Photoactivity Across Entire UV-visible Region for Photoelectrochemical Water Splitting, Nano Lett. 13 (2013) 3817–3823. https://doi.org/10.1021/nl4018385.

[18] A. Naldoni, U. Guler, Z. Wang, M. Marelli, F. Malara, X. Meng, L.V. Besteiro, A.O. Govorov, A.V. Kildishev, A. Boltasseva, V.M. Shalaev, Broadband Hot Electron Collection for Solar Water Splitting with Plasmonic Titanium Nitride, Adv. Optical Mater. 5 (2017) 1601031. https://doi.org/10.1002/adom.201601031.
[19] X. Cheng, S. Gu, A. Centeno, G. Dawson, Plasmonic enhanced Cu2O-Au-BFO photocathodes for solar hydrogen production, Sci. Rep. 9 (2019) 5140. https://doi.org/10.1038/s41598-019-41613-3.
[20] P.S. Archana, N. Pachauri, Z. Shan, S. Pan, A. Gupta, Plasmonic Enhancement of Photoactivity by Gold Nanoparticles Embedded in Hematite Films, J. Phys. Chem. C. 119 (2015) 15506–15516. https://doi.org/10.1021/acs.jpcc.5b02357.
[21] M. Valenti, E. Kontoleta, I.A. Digdaya, M.P. Jonsson, G. Biskos, A. Schmidt-Ott, W.A. Smith, The Role of Size and Dimerization of Decorating Plasmonic Silver Nanoparticles on the Photoelectrochemical Solar Water Splitting Performance of BiVO4 Photoanodes, ChemNanoMat. 2 (2016) 739–747. https://doi.org/10.1002/cnma.201600026.
[22] M.J. Mendes, S. Morawiec, F. Simone, F. Priolo, I. Crupi, Colloidal plasmonic back reflectors for light trapping in solar cells, Nanoscale. 6 (2014) 4796–4805. https://doi.org/10.1039/C3NR06768H.
[23] H. Tan, R. Santbergen, A.H.M. Smets, M. Zeman, Plasmonic Light Trapping in Thin-film Silicon Solar Cells with Improved Self-Assembled Silver Nanoparticles, Nano Lett. 12 (2012) 4070–4076. https://doi.org/10.1021/nl301521z.
[24] H.F. Zarick, W.R. Erwin, A. Boulesbaa, O.K. Hurd, J.A. Webb, A.A. Puretzky, D.B. Geohegan, R. Bardhan, Improving Light Harvesting in Dye-Sensitized Solar Cells Using Hybrid Bimetallic Nanostructures, ACS Photonics. 3 (2016) 385–394. https://doi.org/10.1021/acsphotonics.5b00552.
[25] A. Dabirian, M.M. Byranvand, A. Naqavi, A.N. Kharat, N. Taghavinia, Self-Assembled Monolayer of Wavelength-Scale Core–Shell Particles for Low-Loss Plasmonic and Broadband Light Trapping in Solar Cells, ACS Appl. Mater. Interfaces. 8 (2016) 247–255. https://doi.org/10.1021/acsami.5b08560.
[26] Z. Lu, X. Pan, Y. Ma, Y. Li, L. Zheng, D. Zhang, Q. Xu, Z. Chen, S. Wang, B. Qu, F. Liu, Y. Huang, L. Xiao, Q. Gong, Plasmonic-enhanced perovskite solar cells using alloy popcorn nanoparticles, RSC Adv. 5 (2015) 11175–11179. https://doi.org/10.1039/C4RA16385K.
[27] D. Yang, J.G. Jang, J. Lim, J. Lee, S.H. Kim, J.-I. Hong, Correlations of Optical Absorption, Charge Trapping, and Surface Roughness of TiO2 Photoanode Layer Loaded with Neat Ag-NPs for Efficient Perovskite Solar Cells, ACS Appl. Mater. Interfaces. 8 (2016) 21522–21530. https://doi.org/10.1021/acsami.6b07079.
[28] J. Qi, X. Dang, P.T. Hammond, A.M. Belcher, Highly Efficient Plasmon-Enhanced Dye-Sensitized Solar Cells through Metal@Oxide Core–Shell Nanostructure, ACS Nano. 5 (2011) 7108–7116. https://doi.org/10.1021/nn201808g.
[29] J. Borges, M.S. Rodrigues, C. Lopes, D. Costa, F.M. Couto, T. Kubart, B. Martins, N. Duarte, J.P. Dias, A. Cavaleiro, T. Polcar, F. Macedo, F. Vaz, Thin films composed of Ag nanoclusters dispersed in TiO2: Influence of composition and thermal annealing on the microstructure and physical responses, Appl. Surf. Sci. 358 (2015) 595–604. https://doi.org/10.1016/j.apsusc.2015.08.148.
[30] J. Schou, Physical aspects of the pulsed laser deposition technique: The stoichiometric transfer of material from target to film, Appl. Surf. Sci. 255 (2009) 5191–5198. https://doi.org/10.1016/j.apsusc.2008.10.101.
[31] M. Tian, M. Mahjouri-Samani, G. Eres, R. Sachan, M. Yoon, M.F. Chisholm, K. Wang, A.A. Puretzky, C.M. Rouleau, D.B. Geohegan, G. Duscher, Structure and Formation Mechanism of Black TiO2 Nanoparticles, ACS Nano. 9 (2015) 10482–10488. https://doi.org/10.1021/acsnano.5b04712.
[32] M. Mahjouri-Samani, M. Tian, A.A. Puretzky, M. Chi, K. Wang, G. Duscher, C.M. Rouleau, G. Eres, M. Yoon, J. Lasseter, K. Xiao, D.B. Geohegan, Nonequilibrium Synthesis of TiO2 Nanoparticle "Building Blocks" for Crystal Growth by Sequential Attachment in Pulsed Laser Deposition, Nano Lett. 17 (2017) 4624–4633. https://doi.org/10.1021/acs.nanolett.7b01047.
[33] F. Sauvage, F. Di Fonzo, A. Li Bassi, C.S. Casari, V. Russo, G. Divitini, C. Ducati, C.E. Bottani, P. Comte, M. Grätzel, Hierarchical TiO2 Photoanode for Dye-Sensitized Solar Cells, Nano Lett. 10 (2010) 2562–2567. https://doi.org/10.1021/nl101198b.

[34] J.H. Noh, J.H. Park, H.S. Han, D.H. Kim, B.S. Han, S. Lee, J.Y. Kim, H.S. Jung, K.S. Hong, Aligned Photoelectrodes with Large Surface Area Prepared by Pulsed Laser Deposition, J. Phys. Chem. C. 116 (2012) 8102–8110. https://doi.org/10.1021/jp211233s.

[35] L. Passoni, F. Ghods, P. Docampo, A. Abrusci, J. Martí-Rujas, M. Ghidelli, G. Divitini, C. Ducati, M. Binda, S. Guarnera, A. Li Bassi, C.S. Casari, H.J. Snaith, A. Petrozza, F. Di Fonzo, Hyperbranched Quasi-1D Nanostructures for Solid-State Dye-Sensitized Solar Cells, ACS Nano. 7 (2013) 10023–10031. https://doi.org/10.1021/nn403979h.

[36] B. Yang, M. Mahjouri-Samani, C. M. Rouleau, D. B. Geohegan, K. Xiao, Low temperature synthesis of hierarchical TiO2 nanostructures for high performance perovskite solar cells by pulsed laser deposition, Phys. Chem. Chem. Phys. 18 (2016) 27067–27072. https://doi.org/10.1039/C6CP02896A.

[37] L. Mascaretti, S. Ferrulli, P. Mazzolini, C.S. Casari, V. Russo, R. Matarrese, I. Nova, G. Terraneo, N. Liu, P. Schmuki, A. Li Bassi, Hydrogen-treated hierarchical titanium oxide nanostructures for photoelectrochemical water splitting, Sol. Energy Mater. Sol. Cells. 169 (2017) 19–27. https://doi.org/10.1016/j.solmat.2017.04.045.

[38] M. Ghidelli, L. Mascaretti, B.R. Bricchi, A. Zapelli, V. Russo, C.S. Casari, A. Li Bassi, Engineering plasmonic nanostructured surfaces by pulsed laser deposition, Appl. Surf. Sci. 434 (2018) 1064–1073. https://doi.org/10.1016/j.apsusc.2017.11.025.

[39] J.C. Alonso, R. Diamant, P. Castillo, M.C. Acosta–García, N. Batina, E. Haro-Poniatowski, Thin films of silver nanoparticles deposited in vacuum by pulsed laser ablation using a YAG:Nd laser, Appl. Surf. Sci. 255 (2009) 4933–4937. https://doi.org/10.1016/j.apsusc.2008.12.040.

[40] B.R. Bricchi, M. Ghidelli, L. Mascaretti, A. Zapelli, V. Russo, C.S. Casari, G. Terraneo, I. Alessandri, C. Ducati, A. Li Bassi, Integration of plasmonic Au nanoparticles in TiO2 hierarchical structures in a single-step pulsed laser co-deposition, Mater. Des. 156 (2018) 311–319. https://doi.org/10.1016/j.matdes.2018.06.051.

[41] J.-C. Orlianges, J. Leroy, A. Crunteanu, R. Mayet, P. Carles, C. Champeaux, Electrical and optical properties of vanadium dioxide containing gold nanoparticles deposited by pulsed laser deposition, Appl. Phys. Lett. 101 (2012) 133102. https://doi.org/10.1063/1.4754708.

[42] P. Gondoni, M. Ghidelli, F. Di Fonzo, M. Carminati, V. Russo, A. Li Bassi, C.S. Casari, Structure-dependent optical and electrical transport properties of nanostructured Al-doped ZnO, Nanotechnology. 23 (2012) 365706. https://doi.org/10.1088/0957-4484/23/36/365706.

[43] P. Gondoni, P. Mazzolini, V. Russo, A. Petrozza, A.K. Srivastava, A. Li Bassi, C.S. Casari, Enhancing light harvesting by hierarchical functionally graded transparent conducting Al-doped ZnO nano- and mesoarchitectures, Sol. Energy Mater. Sol. Cells. 128 (2014) 248–253. https://doi.org/10.1016/j.solmat.2014.05.035.

[44] F. Di Fonzo, C.S. Casari, V. Russo, M.F. Brunella, A. Li Bassi, C.E. Bottani, Hierarchically organized nanostructured TiO2 for photocatalysis applications, Nanotechnology. 20 (2009) 015604. https://doi.org/10.1088/0957-4484/20/1/015604.

[45] D. Dominé, F.-J. Haug, C. Battaglia, C. Ballif, Modeling of light scattering from micro- and nanotextured surfaces, J. Appl. Phys. 107 (2010) 044504. https://doi.org/10.1063/1.3295902.

[46] D. Gaspar, A.C. Pimentel, T. Mateus, J.P. Leitão, J. Soares, B.P. Falcão, A. Araújo, A. Vicente, S.A. Filonovich, H. Águas, R. Martins, I. Ferreira, Influence of the layer thickness in plasmonic gold nanoparticles produced by thermal evaporation, Sci. Rep. 3 (2013) 1469. https://doi.org/10.1038/srep01469.

[47] A.B. Tesler, L. Chuntonov, T. Karakouz, T.A. Bendikov, G. Haran, A. Vaskevich, I. Rubinstein, Tunable Localized Plasmon Transducers Prepared by Thermal Dewetting of Percolated Evaporated Gold Films, J. Phys. Chem. C. 115 (2011) 24642–24652. https://doi.org/10.1021/jp209114j.

[48] X. Chen, L. Liu, P.Y. Yu, S.S. Mao, Increasing Solar Absorption for Photocatalysis with Black Hydrogenated Titanium Dioxide Nanocrystals, Science. 331 (2011) 746–750. https://doi.org/10.1126/science.1200448.

[49] A. Naldoni, M. Altomare, G. Zoppellaro, N. Liu, Š. Kment, R. Zbořil, P. Schmuki, Photocatalysis with Reduced TiO2: From Black TiO2 to Cocatalyst-Free Hydrogen Production, ACS Catal. 9 (2019) 345–364. https://doi.org/10.1021/acscatal.8b04068.

[50] S. Kment, F. Riboni, S. Pausova, L. Wang, L. Wang, H. Han, Z. Hubicka, J. Krysa, P. Schmuki, R. Zboril, Photoanodes based on TiO2 and α-Fe2O3 for solar water splitting – superior role of 1D nanoarchitectures and of combined heterostructures, Chem. Soc. Rev. 46 (2017) 3716–3769. https://doi.org/10.1039/C6CS00015K.

[51] M. Altomare, N.T. Nguyen, S. Hejazi, P. Schmuki, A Cocatalytic Electron-Transfer Cascade Site-Selectively Placed on TiO2 Nanotubes Yields Enhanced Photocatalytic H2 Evolution, Adv. Funct. Mater. 28 (2018) 1704259. https://doi.org/10.1002/adfm.201704259.

[52] D. Spanu, S. Recchia, S. Mohajernia, O. Tomanec, Š. Kment, R. Zboril, P. Schmuki, M. Altomare, Templated Dewetting–Alloying of NiCu Bilayers on TiO2 Nanotubes Enables Efficient Noble-Metal-Free Photocatalytic H2 Evolution, ACS Catal. 8 (2018) 5298–5305. https://doi.org/10.1021/acscatal.8b01190.

[53] K.R. Catchpole, A. Polman, Design principles for particle plasmon enhanced solar cells, Appl. Phys. Lett. 93 (2008) 191113. https://doi.org/10.1063/1.3021072.

[54] S.S. Mali, C.S. Shim, H. Kim, P.S. Patil, C.K. Hong, In situ processed gold nanoparticle-embedded TiO2 nanofibers enabling plasmonic perovskite solar cells to exceed 14% conversion efficiency, Nanoscale. 8 (2016) 2664–2677. https://doi.org/10.1039/C5NR07395B.